NANO · MICRO small
www.small-journal.com

Suppression of High Spin State of Mn for the Improvement of Mn-Based Materials in Rechargeable Batteries

Johan Nguyen, Youngil Lee, and Yang Yang**

Manganese-based materials are essential for developing safe, cost-effective, and environmentally sustainable rechargeable batteries, which are critical for advancing clean energy technologies. However, the high spin state of the Mn cation triggers a pronounced Jahn–Teller effect and phase transformations during cycling, leading to structural instability and reduced electrochemical performance of the Mn-based cathodes. This review provides a fundamental understanding of the Jahn–Teller effect, highlights recent strategies to mitigate the high spin state of Mn, and offers insights into future research directions aimed at overcoming the Jahn–Teller effect to enhance the performance of next-generation Mn-based cathodes for rechargeable batteries.

1. Introduction

Manganese-based (Mn-based) electrode materials are central to the development of various rechargeable batteries. These materials utilize the multiple oxidation states of Mn to achieve high redox potential and enable multi-electron transfer, resulting in various types of rechargeable batteries with high specific capacity and energy density.[1–4] Mn-based materials can also be engineered into various derivatives or combined with other elements to form mixed metal compounds, optimizing performance by increasing energy density while maintaining safety and stability.[5–8] In addition, the low cost and non-toxicity of Mn-based materials make them ideal for large-scale production of environmentally sustainable batteries.[9–11] Unfortunately, the existence of Mn^{3+} with a high electron spin state during electrochemical reactions leads to Jahn-Teller distortion, which causes structural degradation, dissolution, migration, and deposition of Mn ions. This ultimately leads to capacity decay and poor cycling stability, which severely limits the practical application of Mn-based materials.[12–16]

The Jahn-Teller effect occurs when molecules or crystals with uneven electron distribution in degenerate orbitals undergo structural distortions.[17–19] In Mn-based materials, this effect is mainly associated with Mn^{3+}, which has an unpaired electron in the e_g orbital.[20,21] This causes significant distortions in the Mn–O octahedra, leading to crystal lattice instability. Such instability adversely affects ionic conductivity and can lead to capacity degradation and shorter cycle life.[14,16,22] The instability is particularly pronounced under non-equilibrium discharge conditions, contributing to mechanical degradation of the material and loss of storage capacity over repeated charge and discharge cycles.[23,24] Given its potential to negatively impact battery performance, the Jahn-Teller effect warrants thorough investigation and strategic management.

Efforts to mitigate the Jahn-Teller effect have led to progress in the development of Mn-based materials for rechargeable batteries, focusing on the partial substitution of Mn by either electrochemically active or inactive transition metal elements, surface engineering, and microstructure design. Despite these achievements, current progress remains insufficient to fully meet practical requirements. Based on a fundamental understanding of the Jahn-Teller effect by reviewing recent strategies to counteract the high spin state of Mn, we offer our perspective on future research directions aimed at further overcoming the spontaneous but notorious Jahn-Teller effect to improve the performance of next-generation Mn-based electrode materials, especially the Mn oxides for monovalent Li-, Na-, and K-ion batteries.

J. Nguyen, Y. Yang
NanoScience Technology Center
University of Central Florida Orlando
Orlando, FL 32826, USA
E-mail: yang.yang@ucf.edu

Y. Lee
Chemical Industry Research Institute
Core Research Institute
University of Ulsan
Ulsan 44776, Republic of Korea
E-mail: nmryil@ulsan.ac.kr

Y. Lee
Department of Chemistry
University of Ulsan
Ulsan 44776, Republic of Korea

Y. Yang
Department of Materials Science and Engineering
University of Central Florida Orlando
Orlando, FL 32826, USA

Y. Yang
Department of Chemistry
University of Central Florida Orlando
Orlando, FL 32826, USA

Y. Yang
Renewable Energy and Chemical Transformation Cluster
University of Central Florida Orlando
Orlando, FL 32826, USA

Y. Yang
The Stephen W. Hawking Center for Microgravity Research and Education
University of Central Florida
Orlando, FL 32826, USA

The ORCID identification number(s) for the author(s) of this article can be found under https://doi.org/10.1002/smll.202410453

DOI: 10.1002/smll.202410453

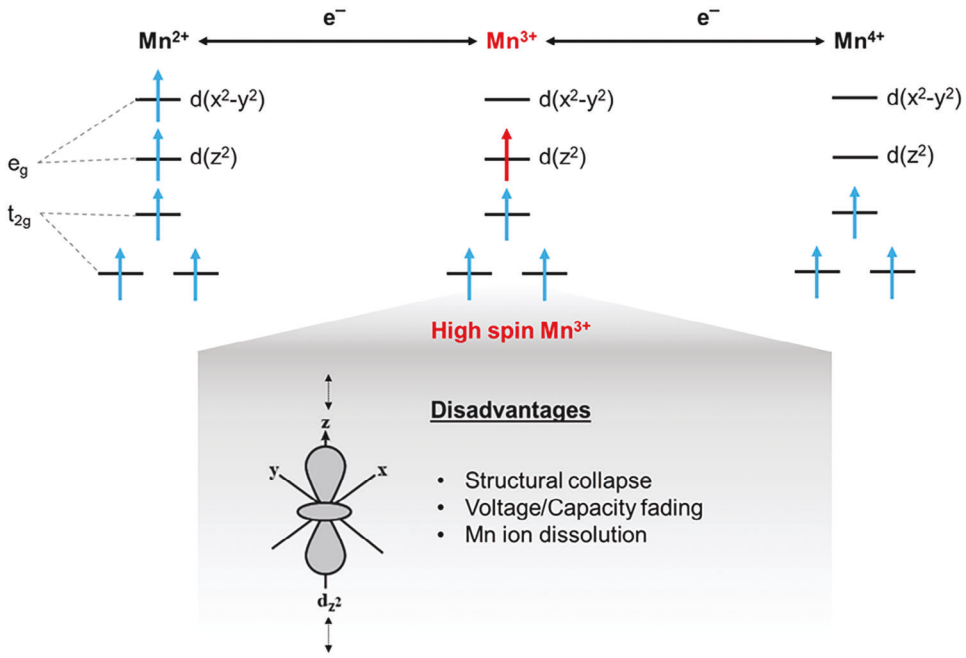

Figure 1. Electron configurations of $Mn^{2+}/Mn^{3+}/Mn^{4+}$. Unlike Mn^{2+} and Mn^{4+}, Mn^{3+} has a single electron that preferentially occupies the $d(z^2)$ orbital, leading to the Jahn–Teller asymmetry distortion of the Mn^{3+} structure which consequently causes the structural collapse, voltage/capacity fading, and Mn ion dissolution of the active materials.

2. High Spin Mn and Jahn–Teller Effect in Mn-Based Cathodes

Although Mn-based electrodes offer significant advantages, several challenges hinder their widespread adoption, particularly due to the coordination structure of Mn in active materials. Manganese, a 3d transition metal with an electron configuration of $3d^5 4s^2$, can exist in various oxidation states in oxides and other compounds.[25] As an electrochemically active center, the electrochemical activity of Mn usually involves Mn^{3+}. Unlike Mn^{2+} and Mn^{4+}, Mn^{3+} has a unique electron configuration of a single electron occupying the e_g orbital. As shown in **Figure 1**, the 3d orbitals are divided into triply degenerate t_{2g} orbitals, including d(xy), d(xz), and d(yz), and doubly degenerate e_g orbitals, including $d(x^2\text{-}y^2)$ and $d(z^2)$. In the high spin state of Mn^{3+}, the single electron in the e_g orbital preferably occupies the $d(z^2)$, creating an asymmetric occupancy state as demonstrated by the differential charge densities of the octahedral $Mn^{3+}O_6$ and $Mn^{4+}O^6$ calculated using the density functional theory (**Figure 2a**).[5] This asymmetry distorts the six equivalent Mn-O bonds, stretching two of them into longer axial bonds and shortening the other four into equatorial bonds. This distortion stabilizes Mn^{3+} but further splits the energy levels of the d-orbitals,[26] leading to crystal distortion, a reduction in system energy, and the elimination of degeneracy in the electronic system. Together, these effects contribute to the challenges of maintaining the structural stability of Mn-based cathodes, thereby limiting their performance in rechargeable batteries.[27,28] The high-spin Mn^{3+} associated with the Jahn-Teller effect plays a vital role in stabilizing Mn-based electrode materials during electrochemical processes. Suppressing the high-spin Mn^{3+} is therefore critical for improving Mn-based materials in rechargeable batteries.

The Jahn-Teller effect significantly influences the phase diversity and stability of Mn-based layered cathodes. In particular, the A-Mn-O systems (A = Li, Na, and K) exhibit a wide range of structural variations that are shaped by the specific A-Mn ratios and synthesis conditions. The planar layered framework of A_xMnO_2 (A = Li, Na, K) can be divided into two primary polymorphs: O-type and P-type, depending on the local environment of the alkali ions, the number and arrangement of the Mn–O layers, and the resulting distorted phases. In this context, O indicates that the alkali ions occupy octahedral sites within the sodium layers, while P indicates prismatic site occupancy.[29] The O-type monoclinic layered structure of $LiMnO_2$ (m-$LiMnO_2$) is of considerable commercial and scientific interest due to its structural similarity to the widely used $LiCoO_2$ cathode material. However, the Jahn-Teller distortion poses a significant challenge as it limits the stability of m-$LiMnO_2$ and promotes the formation of the more thermodynamically stable zigzag layered orthorhombic form (o-$LiMnO_2$).[30] Therefore, the synthesis of m-$LiMnO_2$ is very challenging. Although o-$LiMnO_2$ electrodes initially offer a relatively high capacity of 210 mAh g^{-1}, they suffer from poor capacity retention.[31] During cycling, the layered Li_xMnO_2 rapidly transforms to the spinel phase, driven by the migration of Mn ions into the vacancies left by the extracted Li ions. This phase transition results in an irreversible capacity loss and capacity fading in the ≈3 V region (Figure 2b).[32–34]

The migration of the Mn ion and related charge disproportionation reaction can be further explained by spin integration results as shown in Figure 2c. Considering Li_xMnO_2 with $X_{Li} = 1/2$, the average formal valence state of Mn is +3.5. However, the migrating Mn (octa/tetra face and tetrahedral) has ≈ 4.5 units of electron spin, giving an oxidation state of ~+2.5, indicating that the Mn ion gains d electrons when migrating from octahedral sites to

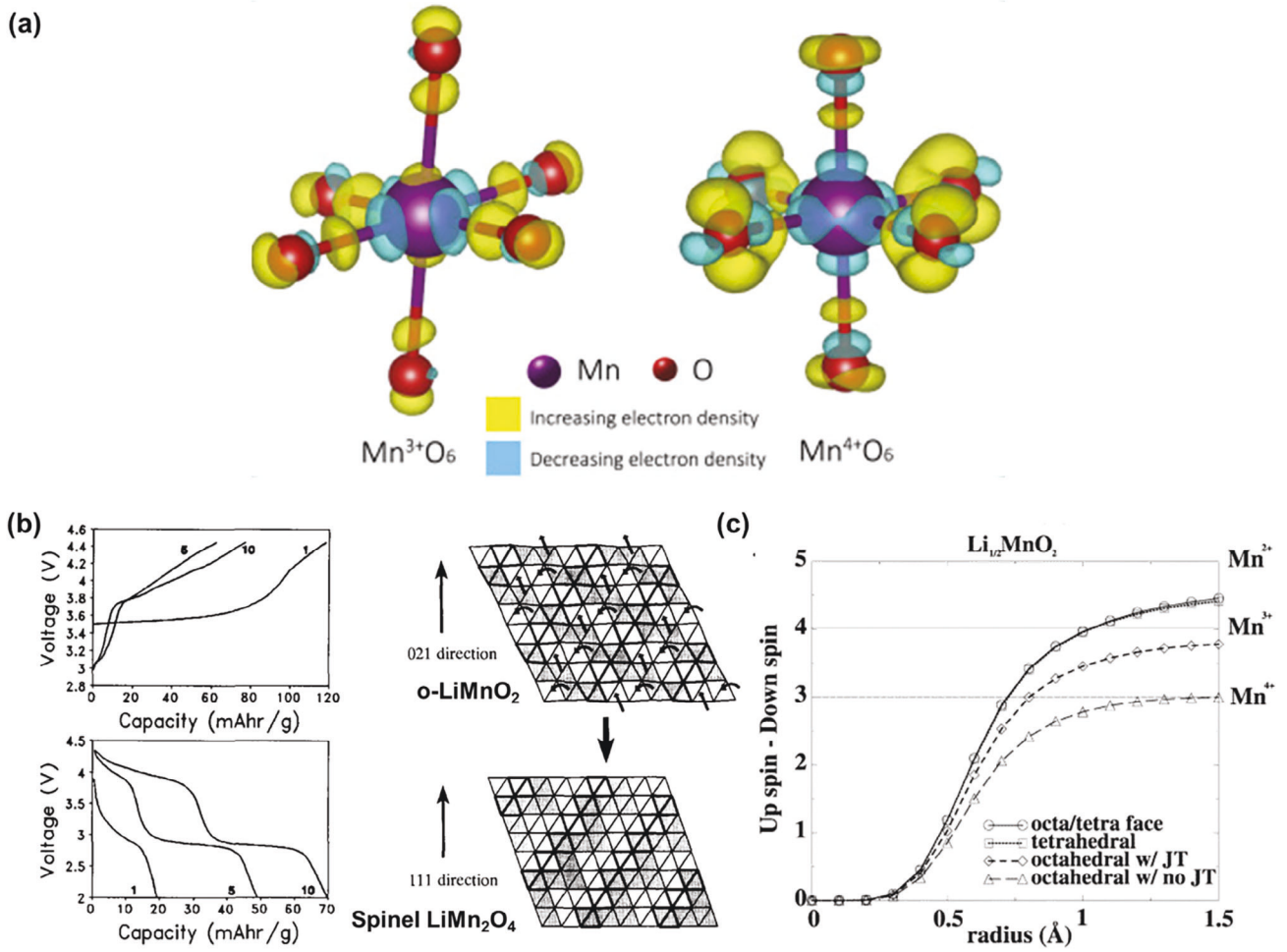

Figure 2. a) The calculated differential charge densities of the octahedral $Mn^{3+}O_6$ and $Mn^{4+}O_6$. Blue and yellow regions represent the decreasing and increasing electron density, respectively. Reproduced with permission from[5] Copyright 2021, Elsevier. c) Typical charge–discharge profiles and schematic diagram of the transformation from o-$LiMnO_2$ to spinel $LiMn_2O_4$. Reproduced with permission from[32] Copyright 1993, Elsevier. d) Integrated net spin for Mn cations from octahedra to tetrahedra path into the Li/vacancy layer at $x_{Li} = ½$. The migrating Mn possesses an oxidation state of ≈+2.5 while Mn in Jahn–Teller-distorted octahedra is ≈+3 and in non-Jahn-Teller-distorted octahedra is +4. The integrated net spin demonstrates that the charge disproportionation reaction induces the migration of Mn between octahedra and tetrahedra. Reproduced with permission from[35] Copyright 2004, American Chemical Society.

tetrahedral vacancies left by the extracted Li ions. Consequently, a neighboring octahedral Mn is oxidized toward +4. It's worth noting that the spontaneous charge disproportionation of Mn^{3+} ($2Mn^{3+}_{(octahedra)} \rightarrow Mn^{2+}_{(tetrahedra)} + Mn^{4+}_{(octahedra)}$) occurs and facilitates the movement of Mn. The amount of Mn^{2+} and the availability of tetrahedral sites are closely related to the Li content in Li_xMnO_2, which further influences the phase stability and performance of the material.[35] In addition, a similar charge disproportionation reaction is reported to occur during the degradation of $Li_xMn_2O_4$ with electrochemical cycling, where the Mn^{2+} dissolves into the electrolyte and then migrates and deposits on the anode, leading directly to the structural degradation of the cathode, the increasing impedance of the anode accompanied with undesired site reactions, and the overall severe capacity degradation of the batteries.[12,13,21]

Even if the layered structure of Li_xMnO_2 could be maintained during cycling, the Jahn-Teller effect would still generate significant mechanical stress, potentially causing the material to fracture. Due to the presence of Mn^{3+}, any methods used to improve the performance of Li_xMnO_2 can only slow down the spontaneous transformation from a layered structure to a spinel phase, but cannot completely prevent it. Once formed, the spinel $LiMn_2O_4$ exhibits a low voltage plateau corresponding to the transformation between cubic $LiMn_2O_4$ and tetragonal $Li_2Mn_2O_4$ (**Figure 3**a).[36] In practical applications, the cycling performance of $LiMn_2O_4$ electrodes is further complicated by these phase transformations and the associated structural distortions in the low-voltage region. As a result, the operating voltage range of $LiMn_2O_4$ is limited (Figure 3b,c).[37,38] The structural mismatch between the tetragonal and cubic phases disrupts the Li-ion diffusion pathways, resulting in sluggish kinetics and capacity degradation over repeated cycles. In addition, during lithiation of the spinel $LiMn_2O_4$, a high concentration of Mn^{3+} accumulates at the surface during discharge. This triggers a

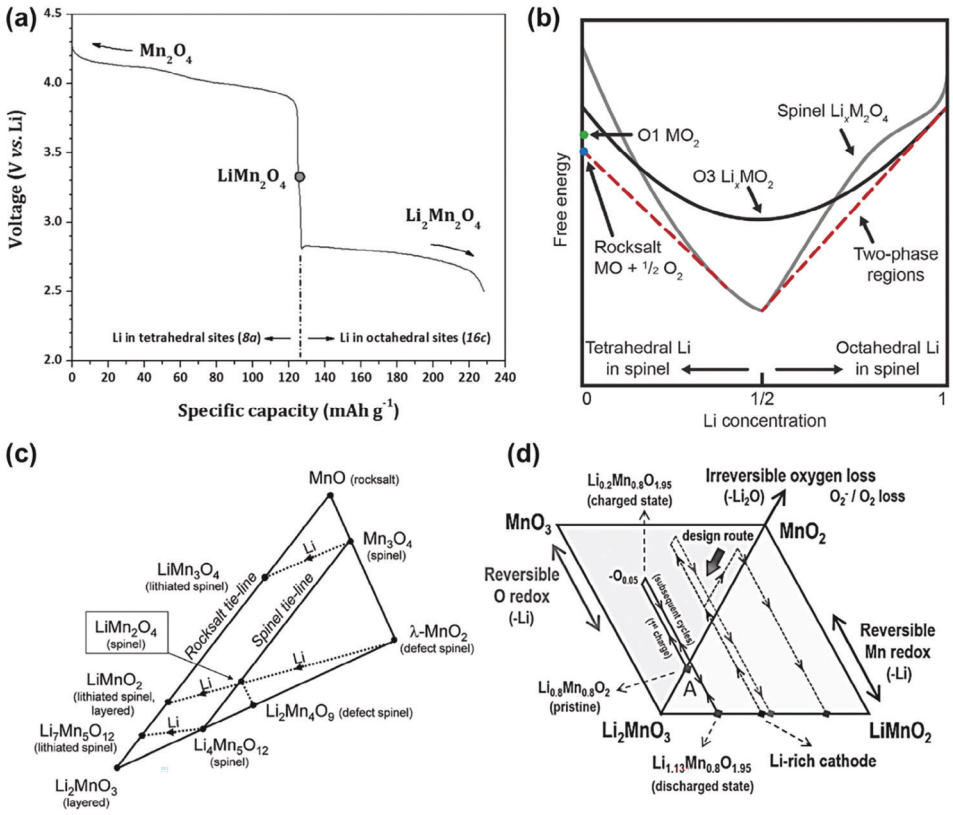

Figure 3. a) Voltage profile of $LiMn_2O_4$ during cycling. Reproduced with permission from[36] Copyright 2013, American Chemical Society. b) Schematic free energy curves of O-type layered Li_xMO_2 and spinel $Li_xM_2O_4$. The material can be fully charged to MO_2 and ideally could then be reversibly discharged back to the original $LiMO_2$ state. However, the process may result in atomic rearrangement to spinel LiM_2O_4 or to rocksalt MO. Reproduced with permission from[37] Copyright 2017, John Wiley and Sons. c) Compositional Li-Mn-O phase diagram concerning spinel, rock salt, and layered compounds. Reproduced with permission from[38] Copyright 2018, Royal Society of Chemistry. d) Compositional phase diagram showing the electrochemical reaction pathways for Li-rich Mn-based cathodes. Reproduced with permission from[45] Copyright 2020, John Wiley and Sons.

disproportionation reaction that causes continuous dissolution of Mn^{2+} ions into the electrolyte, further degrading the battery performance over time.[39,40]

Beyond the Li deficient spinel $LiMn_2O_4$, Li ions can replace Mn, leading to the formation of $(LiMn_2)$-O sheets. These sheets help to maintain a layered structure but distort the original lattice symmetries, resulting in the formation of Li-rich Li_2MnO_3 cathodes.[38,41] However, the Li-O-Li configurations lead to the formation of non-bonding O orbitals, which lower the average valence of Mn and can cause electron loss from oxygen, thereby intensifying the Jahn-Teller effect.[42,43] This, in turn, triggers interplanar and intraplanar displacements of various metal ions, leading to voltage hysteresis and capacity reduction.[44] The compositional phase diagram of a typical Li-rich Li_2MnO_3 cathode can be extended to the Li_2MnO_3-$LiMO_2$-MnO_2-MnO_3 configuration by including the MnO_3 region (Figure 3d).[45] This diagram shows both reversible (in the Li_2MnO_3-MnO_2-MnO_3 direction) and irreversible (in the Li_2MnO_3-$LiMnO_2$-MnO_2 direction) phase transformations. These transformations and separations induce significant volumetric strain in the bulk material, leading to repeated volume changes and crack formation. As a result, these structural changes reduce the electrochemical reversibility of the active materials and hinder the long-term performance of Li-rich Mn-based cathodes.[46]

Unlike their Lithium counterparts, where even small deviations from x = 1 can induce structural transformation to a spinel phase, the planar layered framework for Na_xMnO_2 remains relatively stable over a wide range of x values.[47,48] As shown in **Figure 4a**, the Na ion diffusion in P-type Na_xMnO_2 is generally less complex than in O-type structures due to the presence of more direct diffusion pathways with lower hopping energies between adjacent Na sites.[47] In P-type phases, Na ions occupy trigonal prisms that share rectangular faces, creating a direct pathway that facilitates Na ion diffusion and enhances reversible Na ion intercalation. In contrast, a Na ion moves from one octahedral environment to another equivalent one by crossing an octahedral-tetrahedral face in O-type phases, resulting in a relatively high activation barrier. However, despite the improved Na-ion diffusion in P-type structures, the low initial Na content of these layered oxides raises concerns about sodium deficiency, which could pose a challenge for practical full-cell assembly.

It should be noted that orthorhombic zigzag-type layered $NaMnO_2$ exists with edge-sharing MnO_6 octahedra that induce Na ions to reside in the intermediate sites.[49,50] As shown in Figure 4b, the basic planar layered framework of Na_xMnO_2

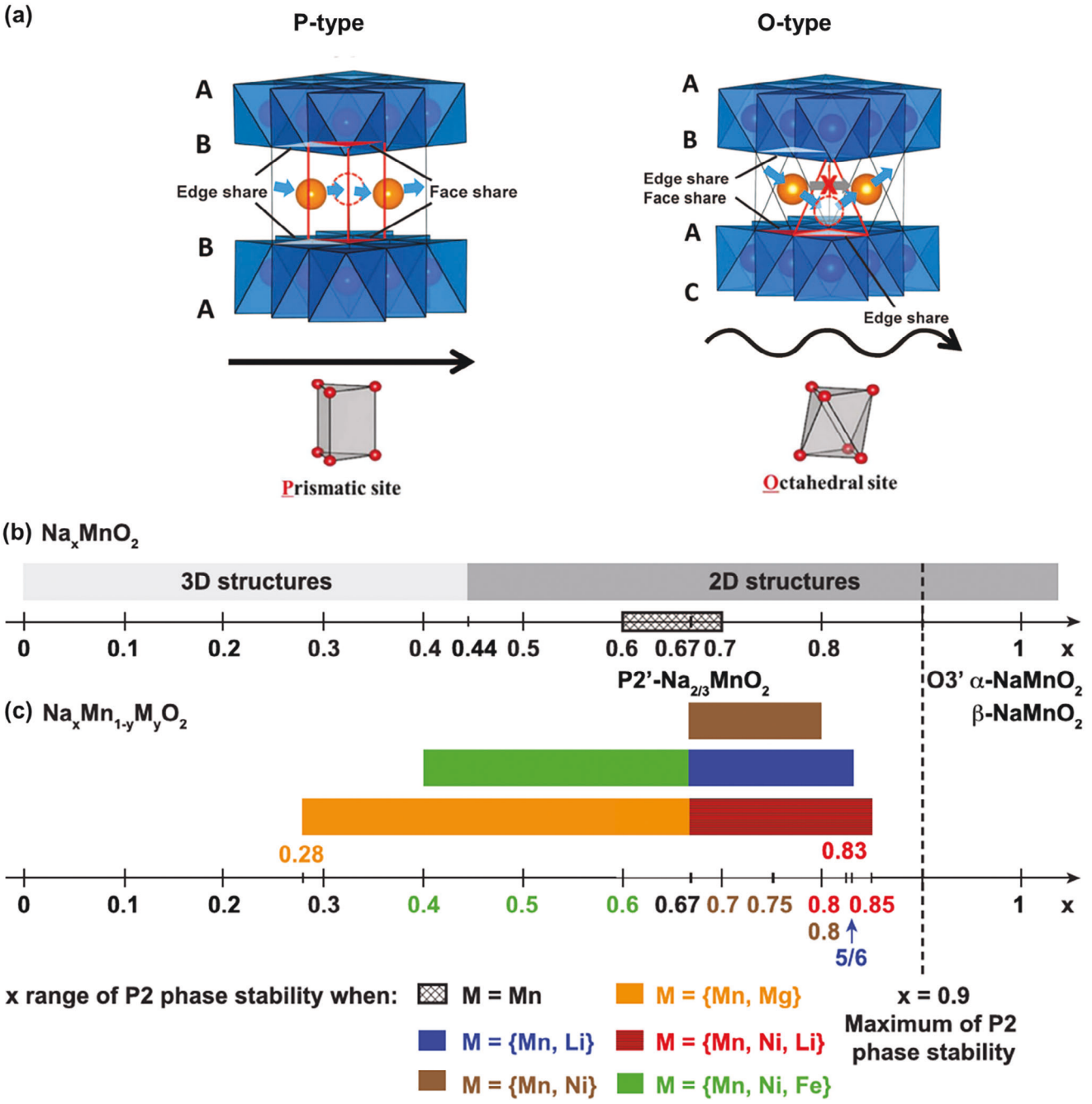

Figure 4. a) Typical P- and O-type of Na_xMnO_2 with corresponding Na-ion diffusion path. Reproduced with permission from[47] Copyright 2014, American Chemical Society. Ranges of x in b) Na_xMnO_2 and c) $Na_xMn_{1-y}M_yO_2$ for different layered structures. Reproduced with permission from,[51] under the terms of the Creative Commons Attribution 4.0 License.

exhibits a P-type structure when x is in the range of 0.6-0.7, and transitions to an O-type structure as x approaches 1.[51,52] The incorporation of various elements into this framework can modify the x range while maintaining the P-type structure, as shown in Figure 4c. Transition metal substitution is an effective way to increase the Na content in the P2-type phases as high as ≈0.85 by partial substitution of Mn for Ni, Li, or a combination of both[53] but it requires a relatively lower upper cutoff voltage to prevent structural changes and thus just moderately improve the reversible capacities.

Similar to the Jahn-Teller effect in Li-ion batteries, these structural dynamics in Mn-based cathodes for Na- and K-ion batteries underscore the need for careful consideration of phase stability and ion diffusion pathways to optimize battery performance. In O-type Na_xMnO_2, the higher Na content allows for a higher initial discharge capacity, making it more promising for practical applications. However, the charge-discharge curves often show

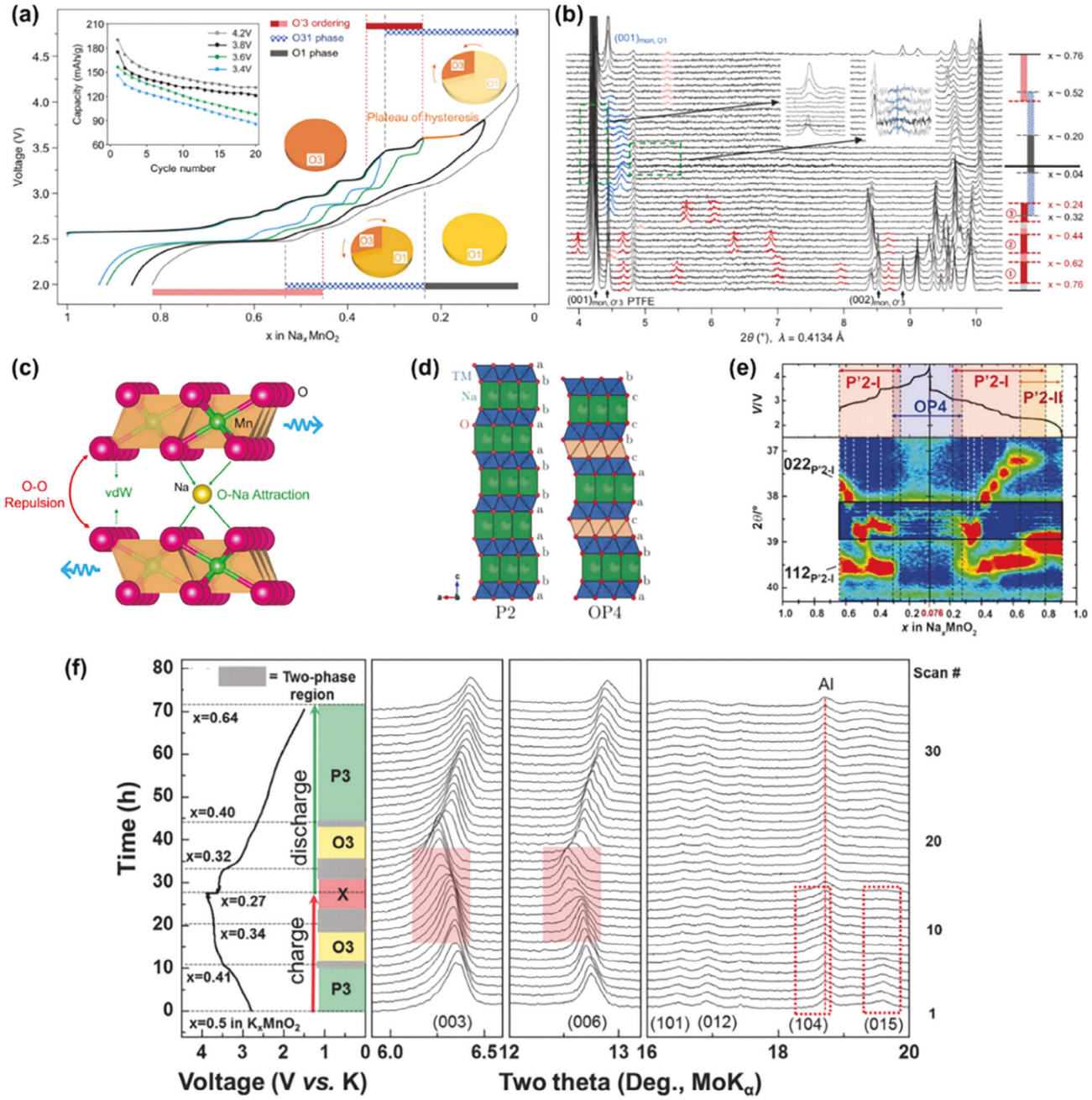

Figure 5. a) Electrochemical performance and complicated structural evolution of O-type $NaMnO_2$ based on b) in situ synchrotron XRD in the first electrochemical cycle. Reprinted with permission from[55] Copyright 2018, John Wiley and Sons. c) Schematic illustration of interlayer gliding. Reproduced with permission from[57] Copyright 2022, American Chemical Society. d) The P2 and OP4 crystal structures. Reproduced with permission from[71] Copyright 2023, John Wiley and Sons. e) Structural distortion and P–O transformation of P-type $Na_{2/3}MnO_2$ based on contour maps of operando XRD patterns. Reproduced with permission from[59] Copyright 2016, John Wiley and Sons. f) Typical charge–discharge profiles of P3-type $K_{0.5}MnO_2$ and corresponding in situ XRD pattern, showing the structural changes of the P3-type $K_{0.5}MnO_2$ during charge and discharge with the formation of unknown X-phase. Reprinted with permission from[66] Copyright 2017, John Wiley and Sons.

multiple voltage steps, indicating complex phase transitions as presented in **Figure 5**a,b.[54,55] These undesirable phase transitions during cycling can lead to irreversible structural changes and rapid degradation of electrochemical performance. As illustrated in Figure 5c, the Mn–O sheets in P-type Na_xMnO_2 slide within the a–b plane to prevent close oxygen–oxygen contact during Na extraction, resulting in different imperfect layered structures with stacking defects.[56,57] This induces P-type distortions and P–O transformations in both Mn-redox active and Mn-redox inert oxides (Figure 5d,e).[58–61] The irreversible structural

transformation, coupled with the large volume change during cycling, raises serious concerns about the cycle stability of the Mn-based electrodes.[62–65] Although it has been commonly observed that the structural instability leads to oxygen layer glides at high voltage at the end of charge, the resulting phases are usually difficult to ascertain because of the extensive disorder and the formation of stacking faults can broaden the peaks in the diffraction patterns. For K-ion intercalation in Mn-based layered electrodes, the P–O phase transition is accompanied by the formation of an unknown phase (X) (Figure 5f).[66] While spinel phase formation is favorable in $LiMnO_2$ and energetically less favorable in $NaMnO_2$,[22] a dual interphase layer consisting of a spinel interlayer of inactive Mn_3O_4 and a solid-electrolyte interphase film can still form on the surface of P-type $K_{0.67}MnO_2$ active particles.[67] It should be noted that the larger radius of K ions poses a significant challenge to the transport of K ions within K_xMnO_2 materials thus reducing the value of x in thermodynamic stable P-type K_xMnO_2 and inducing more severe structural changes and distortions.[68–70] This results in a significant decrease in power density, underscoring the complexity of developing K-ion batteries.

3. Suppression of High Spin Mn in Mn-Based Cathodes

The capacity decay in layered Mn-based materials for rechargeable batteries is closely linked to the Jahn-Teller distortion associated with the high-spin electron configuration of Mn^{3+} and the resulting charge disproportionation. These undesirable phase transformations during cycling often lead to irreversible structural changes and rapid degradation of electrochemical performance, presenting significant challenges for Mn-based cathodes. The extent of the structural change is highly associated with the degree of Mn^{3+} involved in the redox reactions. To enhance the electrochemical stability, a key strategy is to suppress the high-spin state of Mn^{3+}, thereby mitigating the Jahn-Teller effect and the complex structural transformations that occur during the electrochemical process. Modulating the electron configuration of Mn is essential in this context. Chemical substitutions offer a powerful approach to influencing the valence state of Mn, particularly in its tetrahedral or octahedral sites. A series of first-principles calculations have demonstrated the effect of a variety of chemical substitutions on the valence of Mn and how this in turn affects the electron configuration of Mn.[72–74] Reed and Ceder[35] suggested that a strong preference by Mn for octahedral over tetrahedral coordination should result in reduced mobility for Mn. A reduced mobility for Mn in turn could increase the resistance of metastable chemically substituted Mn oxide structures against structural transformation. Their calculations revealed that the substitution of Mn by low fixed valence cations (Li^+, Mg^{2+}, Al^{3+}) and electronegative multivalent cations (Co^{3+}, Ni^{2+}, Cu^{2+}) that oxidize Mn^{3+} ($Mn^{3+} \rightarrow Mn^{4+}$) stabilize Mn in the octahedral sites while other elemental substitutions with Zr^{4+}, Sn^{4+}, V^{5+} can destabilize the layered structure (**Figure 6a**). By predicting the effects of these substitutions, it is possible to maintain Mn in a relatively stable +4 valence state throughout the electrochemical cycle, ultimately reducing structural distortions and enhancing battery performance.

Modulating electronic and crystal structures of Mn-based cathodes by elemental doping and substitution becomes the most extensive approach to improve the basic physical properties of the active materials, leading to extensive theoretical and experimental research on various Mn combinations as widely reported and reviewed.[5,6,68,69,75–77] The effectiveness of elemental substitution and vacancy formation lies primarily in their ability to inhibit Jahn-Teller distortion by adjusting the Mn–O–*Sub* electron configuration and lattice parameters. This not only improves structural stability but also creates favorable ion diffusion pathways. In addition, the Mn–O–*Sub* bond can increase the spacing between alkali metal layers, reduce Coulombic interactions in layered oxides, and suppress undesirable phase transformations, all of which contribute to improved electrochemical performance. The cationic disordering, including excessive Li at Mn sites and Li/Mn exchange, in a Mn spinel material can intrinsically suppress the Jahn-Teller distortion of $Mn^{3+}O_6$ octahedrons by breaking the symmetry of Mn^{3+} arrangements to disrupt the correlation of distortions arising from individual Jahn-Teller centers and prevent the Mn^{3+}–O bonds distorting along one direction and even make them counteract with each other. As a result, a double capacity (≈240 mAh g^{-1}) can be accessed for the disordered materials with good reversible cycling stability.[78] Replacing Mn with smaller radius ions can result in a contracted crystal lattice and microstrains due to the shorter and stronger *Sub*–O bond compared to Mn–O. In contrast, larger radius ions are expected to expand the lattice parameters, facilitating the free movement of charged ions within the oxide and potentially increasing the rate capability. In addition, the incorporation of inert cations such as Mg^{2+} and Al^{3+} primarily serves to stabilize the Mn–O layers, while the combination of Mn with other redox-active elements can fundamentally alter its electrochemical properties, leading to improved battery performance.

The calculated qualitative ionization energies for different 3d ions provide insight into predicting substitutions that can stabilize octahedral Mn in a relatively immobile valence state (near +4) throughout the electrochemical cycle, as presented in Figure 6b. Adequate substitution of Mn can lead to the formation of inactive Mn^{4+} as observed for $LiNi_{0.5}Mn_{0.5}O_2$ in which it is generally understood that both Ni and Mn should have an average valence of +3. However, since $Mn_{(oct)}^{3+\rightarrow 4+}$ is lower than $Ni_{(oct)}^{2+\rightarrow 3+}$, Mn^{3+} is more likely to be oxidized to Mn^{+4} by the reduction of $Ni_{(oct)}$ from 3+ to 2+, resulting in the existence of inactive Mn^{4+} in $LiNi_{0.5}Mn_{0.5}O_2$.[79,80] The inactive Mn^{4+} has been observed in various Mn-based electrodes, showing better cycling stability although it may partially reduce the initial discharge capacity of the active materials.[81–83] As demonstrated in **Figure 7a**, the Mn average valence was also regulated by partial substitution of Mn with Ti^{4+} and Mg^{2+} ions. While the introduction of Ti^{4+} ions reduced the valence of Mn, the Mg^{2+} ions increase the Mn valence. According to the measured results combined with the calculation of the charge compensation mechanism, the Mn average valence in $K_{0.5}Mn_{0.7}Co_{0.2}Fe_{0.1}O_2$, $K_{0.5}Mn_{0.6}Co_{0.2}Fe_{0.1}Ti_{0.1}O_2$, and $K_{0.5}Mn_{0.6}Co_{0.2}Fe_{0.1}Mg_{0.1}O_2$ are +3.714, +3.667, and +4, respectively. The e_g orbitals of Mn in $K_{0.5}Mn_{0.6}Co_{0.2}Fe_{0.1}Mg_{0.1}O_2$ is not split, implying that the Mn (+4) is Jahn–Teller inactive. The $K_{0.5}Mn_{0.6}Co_{0.2}Fe_{0.1}Mg_{0.1}O_2$ cathode exhibits outstanding cycling stability with capacity retention of 91% at 0.1 A g^{-1} after 150 cycles, and retained 74% of the initial capacity even after

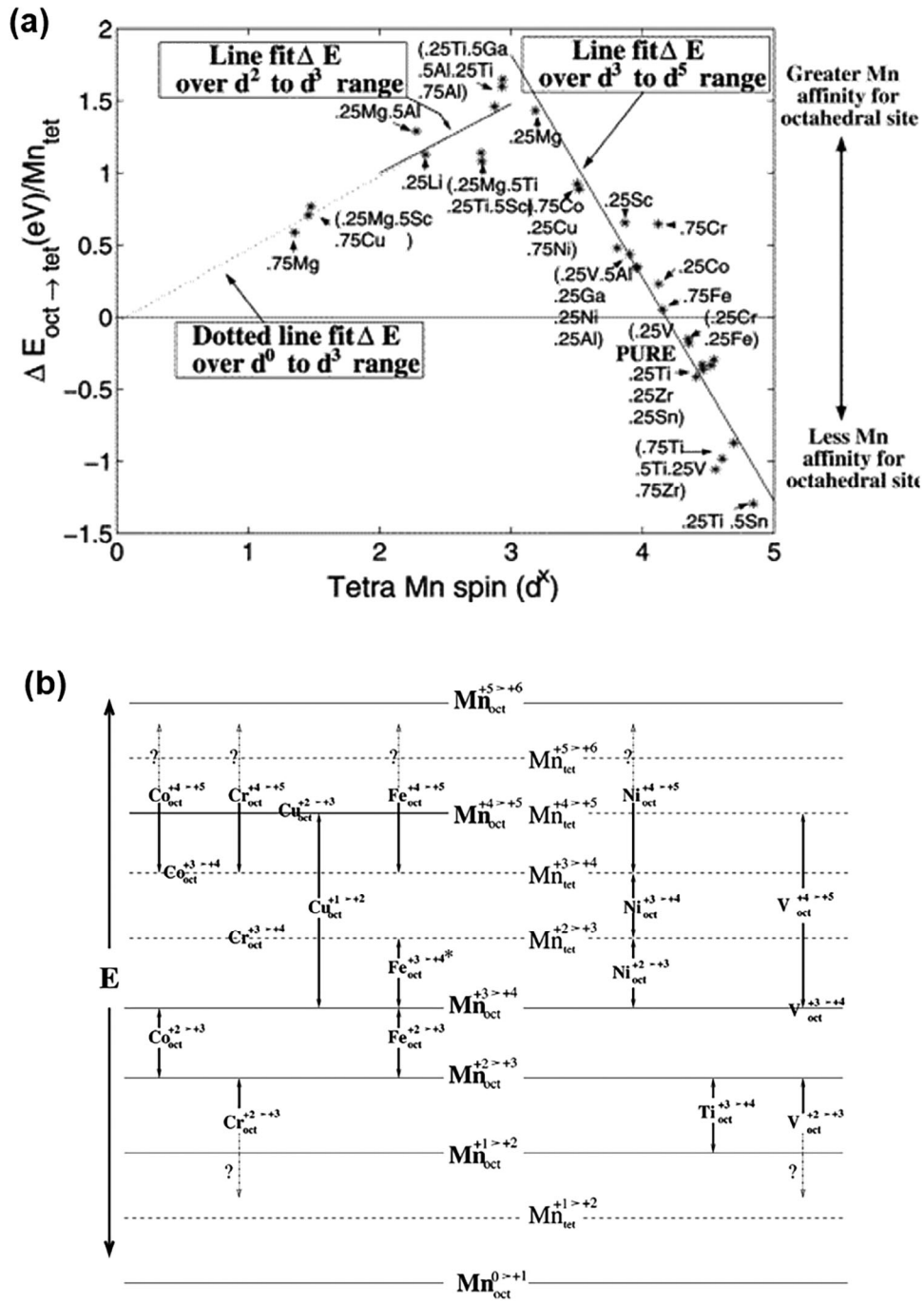

Figure 6. a) Energy difference of different Mn substitutions with and without tetrahedral Mn, showing the tendency to migrate between octahedral and tetrahedral sites of Mn under the effects of different substitutions. b) Qualitative ionization energies for 3d ions at various valences in an oxide framework, in comparison with Mn ionization energies in octahedra and tetrahedra coordination labeled prominently in the center of the figure. Reprinted with permission from[35] Copyright 2004, American Chemical Society.

500 cycles at 1 A g^{-1}. Overall electrochemical properties of the active materials are now dominantly generated by the substituted elements, making it crucial to thoroughly investigate the stability of these substitutions. For example, electrochemically active elements used for the substitution of Mn such as Fe and Cr may also exhibit Jahn-Teller distortions in certain oxidation states during cycling.[84,85] Nevertheless, the strategy shown in Figure 6b effectively predicts the valence of two or more substituted ions coexisting in a stable oxide and offers a promising approach to designing high-capacity cathodes with multiple ion coexistence, as seen in the stable range of P-type $Na_xMn_{1-y}M_yO_2$ shown in Figure 4c.

Suppressing the Jahn-Teller effect is not limited to cation substitutions; it can also be achieved through anion substitutions at the –O sites. Replacing –O with mono atoms such as

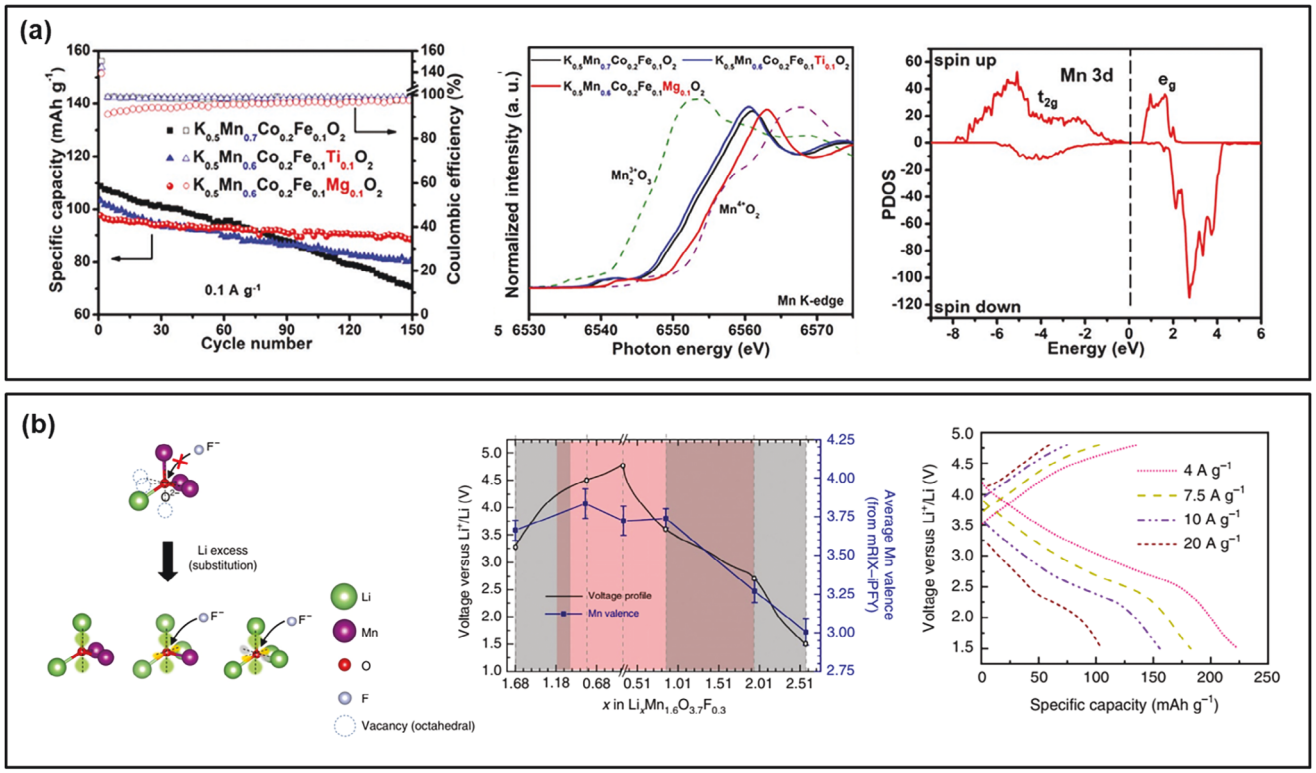

Figure 7. a) Cycling property of $K_{0.5}Mn_{0.7}Co_{0.2}Fe_{0.1}O_2$, $K_{0.5}Mn_{0.6}Co_{0.2}Fe_{0.1}Ti_{0.1}O_2$, and $K_{0.5}Mn_{0.6}Co_{0.2}Fe_{0.1}Mg_{0.1}O_2$ and their XANES spectra of Mn K-edge. Notably, XANES spectra show that the average oxidation state of Mn in $K_{0.5}Mn_{0.6}Co_{0.2}Fe_{0.1}Mg_{0.1}O_2$ is close to +4. The partial density of states of Mn 3d electronic orbital in $K_{0.5}Mn_{0.6}Co_{0.2}Fe_{0.1}Mg_{0.1}O_2$ shows that the e_g orbitals are unoccupied, revealing the existence of Jahn–Teller inactive Mn^{4+}. Reproduced with permission from[83] Copyright 2021, John Wiley and Sons. b) Change in the local bonding environment of anions from a stoichiometric spinel to a Li-excess spinel with Florine substitution. Quantification of Mn redox reactions in $Li_xMn_{1.6}O_{3.7}F_{0.3}$ during the initial cycle shows the adaption of the Mn oxidation state during cycling. The galvanostatic voltage profiles of $Li_xMn_{1.6}O_{3.7}F_{0.3}$ at high current rates exhibit high-capacity delivery of the F-substituted material. Reprinted with permission from[94] Copyright 2020, Springer Nature.

–S, –F, or polyanion groups like $–BO_3$ and $–PO_4$ directly affects the electron configuration and coordination of Mn centers. This substitution alters the M–O/*Sub* bond through inductive effects, typically resulting in changes in bond spacing and ionicity, which in turn affect electron conductivity and electrochemical potential.[86,87] Among different –O site substitutions, the introduction of –F, a more electronegative element, can drive phase transformations toward more thermodynamically stable structures, lower the energy barrier for alkali ion intercalation, and create additional active sites for ion storage.[88–93] As shown in Figure 7b, F substitution combined with compositional adjustment from Li-rich $Li_{1.28}Mn_2O_4$ to $Li_{1.68}Mn_{1.6}(O, F)_4$ significantly increases the kinetically accessible Li capacity, enabling both high energy density and excellent rate capability in Li-ion spinel battery cathodes.[94] Since the theoretical Mn capacity is only 178 mAh g^{-1} in $Li_{1.68}Mn_{1.6}(O, F)_4$, a significant portion of the observed capacity at 4 A g^{-1} is still expected to originate from reversible O redox which is stabilized and facilitated by the lack of Mn migration. It should be noted that although the presence of F does not completely eliminate the high-spin state of Mn, fine-tuning the degree of fluorination along with structural transformation and electrochemical performance provides valuable insights from both atomic and molecular perspectives.

In addition to the introduction of dopants or substitution, modulation of the electronic and crystal structures of Mn-based cathodes can also be achieved through the development of sophisticated gradient, disordered, vacancy-matched Mn^{3+}, and integrated phase, core-shell structures, or a combination of these approaches.[56,95–99] For example, the microstructure design with interwoven spinel and layered domains has provided new insights into the elimination of the Jahn-Teller effect for a $LiMnO_2$ cathode. At the interface between these two domains, the Mn $d(z^2)$ orbitals are oriented perpendicular to each other, resulting in an interfacial orbital order that suppresses the Jahn-Teller distortion and the consequent Mn dissolution. As a result, the heterostructured cathode offers improved structural and electrochemical cycling stability as providing a high Li storage capacity of 254.3 mAh g^{-1} and unprecedented cyclability with ≈90.4% capacity retention after 2000 cycles.[95] By introducing vacancies into the transition metal layer of P2-$Na_{0.7}Fe_{0.1}Mn_{0.75}\square_{0.15}O_2$ ("□" represents a vacancy), the transition metal vacancy serves to suppress Na ion migration to maintain structural and thermal stability in Na-depleted states and to trigger a reversible anionic redox reaction to increase the energy density. As a result, the designed cathode enables pouch cells with energy densities of 170 Wh kg^{-1} and 120 Wh kg^{-1} which can operate for over 600 and 1000 cycles, respectively.[99] In another work, a double-layer phosphate of

$K_3PO_4/MnPO_4$-coated $K_{0.5}Mn_{0.8}Co_{0.2}O_2$ cathodes shows a higher electron and K-ion conductivity, less surficial oxygen loss and layered-to-spinel-to-rock salt tri-phase transition, and less internal lattice expansion and contraction during cycling. In addition, first principles calculations imply that the surface modification can effectively prevent Mn ions dissolution and oxygen release. The coated materials exhibit a highly reversible specific capacity (101.3 mAh g^{-1} at 0.1 A g^{-1}) and excellent rate performance and capacity retention of 80% after 500 cycles at 1 A g^{-1} compared to uncoated one (78.6 mAh g^{-1} at 0.1 A g^{-1} with 67.3% capacity retention).[100] Engineering bulk particles are particularly effective in stabilizing the structure through mutual effects between adjacent atoms or layers, while surface modifications are very useful to resist Mn dissolution in the electrolyte and protect the electrode materials. Despite these efforts, phase transformation in Mn-based cathodes is unlikely to be eliminated when the Mn ions remain in the +3 state throughout the cycling process. By carefully controlling the reaction parameters and utilizing multiple synthetic routes, it is expected to tailor the Mn-based electrode materials with desired compositional stoichiometry and particle morphology with crystal phase stability to improve their electrochemical properties for practical applications.

4. Conclusion and Outlook

Mn-based materials have shown great potential in the field of energy storage. However, their practical application has been limited by the nature of Mn^{3+} with high-spin electron configuration. The electron distribution in Mn^{3+} causes the Jahn-Teller distortions and charge disproportionation, leading to the complexity of Mn structures and inducing the spontaneous and thermodynamically driven regulation of Mn valence during the electrochemical cycling. Considerable efforts have been made to theoretically predict the structural stability based on the compositional material design, and then to experimentally investigate the designed structures. The resistance to crystal transformation of metastable compounds depends on the relative stability of Mn in octahedral coordination. Approaches to suppress the violent Jahn-Teller effect, therefore, have focused on substitution and/or doping of heterogeneous atoms in the bulk to manipulate the average valence of Mn, as well as on structural designs to control the electrochemical properties of the active materials from the surface to the core. To date, the intrinsic Jahn-Teller distortion and the resulting phase transformation remain a major challenge for the practical application and commercial widespread use of Mn-based materials.

Future studies on the suppression of the Jahn-Teller effect in Mn-based active materials will require the incorporation of material design, controlled synthesis, and functionalization, advanced real-time characterization techniques, and accurate theoretical calculations. Since there is a dilemma in choosing between maximizing alkali ion content for high-capacity cathodes and relatively lower alkali ion content for more stable and faster ion-conducting active materials, as observed for the O- and P-type layered electrodes, these factors will serve as key techniques to bridge charge density and structural stability. Since Mn^{4+} is the most stable valence, it may be desirable to electrochemically cycle Mn between elevated oxidation states centered closer to +4 rather than across the +3/+4 redox range. However, a significant loss of capacity due to the inactive Mn^{4+} must be considered. Although Mn has valences higher than +4, the lack of electrolytes that can withstand the oxidative strength of Mn at such high valences becomes the bottleneck issue.

It should be noted that material design combined with theoretical calculations can predict the electrochemical potential of the electrode at which the material will (de)intercalate charged ions. Increasing the electrochemical potential of the positive electrode material is necessary to increase the energy density of the energy storage systems. In addition, real-time monitoring through advanced characterization techniques can detect some non-equilibrium within short intermediate states to elucidate the complex phase stability of the Mn-based compounds, providing an in-depth understanding of the reaction mechanism, structure-performance relationships, and active material degradation for further development. Finally, achieving high ionic and electronic conductivity materials and limiting the interfacial/interphase side reactions will narrow the gap between theoretical investigation and practical applications of Mn-based cathodes for rechargeable batteries.

Acknowledgements

This work was supported by the National Science Foundation under Grant CBET-1949840 and ACS PRF (65481-ND10). J.N. acknowledges the financial support from the Preeminent Postdoctoral Program (P3) at UCF. Y.L. acknowledges the National Research Foundation of Korea (NRF) grant funded by the MSIT (2021R1A2C1010373) and the MOE (2021R1A6A1A03038858 and 2022R1A6C101C732).

Conflict of Interest

The authors declare no conflict of interest.

Author Contributions

All authors wrote, reviewed, and revised the paper.

Keywords

cycling performance, Jahn–Teller effect, lithium-ion batteries, Mn-based cathodes, phase transformations

Received: November 5, 2024
Revised: December 9, 2024
Published online:

[1] N. Nitta, F. Wu, J. T. Lee, G. Yushin, *Mater. Today* **2015**, *18*, 252.
[2] J. Lee, D. A. Kitchaev, D.-H. Kwon, C.-W. Lee, J. K. Papp, Y.-S. Liu, Z. Lun, R. J. Clément, T. Shi, B. D. McCloskey, J. Guo, M. Balasubramanian, G. Ceder, *Nature* **2018**, *556*, 185.
[3] Y. S. Moghadam, A. El Kharbachi, T. Diemant, G. Melinte, Y. Hu, M. Fichtner, *Chem. Mater.* **2021**, *33*, 8235.
[4] H. Hu, H.-C. He, R.-K. Xie, C. Cheng, T. Yan, C. Chen, D. Sun, T.-S. Chan, J. Wu, L. Zhang, *Nano Energy* **2022**, *99*, 107390.
[5] S. Liu, B. Wang, X. Zhang, S. Zhao, Z. Zhang, H. Yu, *Matter* **2021**, *4*, 1511.

[6] H. Li, W. Zhang, K. Sun, J. Guo, K. Yuan, J. Fu, T. Zhang, X. Zhang, H. Long, Z. Zhang, Y. Lai, H. Sun, *Adv. Energy Mater.* **2021**, *11*, 2100867.
[7] N. Zhang, J.-C. Wang, Y.-F. Guo, P.-F. Wang, Y.-R. Zhu, T.-F. Yi, *Coord. Chem. Rev.* **2023**, *479*, 215009.
[8] X. Zhao, X. Cao, H. Zhou, *Acc. Mater. Res.* **2024**, *5*, 307,.
[9] W. Zuo, A. Innocenti, M. Zarrabeitia, D. Bresser, Y. Yang, S. Passerini, *Acc. Chem. Res.* **2023**, *56*, 284.
[10] H. Yi, Y. Liang, Y. Qian, Y. Feng, Z. Li, X. Zhang, *Batteries* **2023**, *9*, 246.
[11] J. Xiao, F. Shi, T. Glossmann, C. Burnett, Z. Liu, *Nat. Energy* **2023**, *8*, 329.
[12] C. Zhan, T. Wu, J. Lu, K. Amine, *Energy Environ. Sci.* **2018**, *11*, 243.
[13] T. Liu, A. Dai, J. Lu, Y. Yuan, Y. Xiao, L. Yu, M. Li, J. Gim, L. Ma, J. Liu, C. Zhan, L. Li, J. Zheng, Y. Ren, T. Wu, R. Shahbazian-Yassar, J. Wen, F. Pan, K. Amine, *Nat. Commun.* **2019**, *10*, 4721.
[14] A. R. Armstrong, P. G. Bruce, *Nature* **1996**, *381*, 499.
[15] Y. Shao-Horn, S. A. Hackney, A. J. Kahaian, K. D. Kepler, E. Skinner, J. T. Vaughey, M. M. Thackeray, *J. Power Sources* **1999**, *81–82*, 496.
[16] T. Liu, S. Hou, Y. Li, S. Xue, J. Hu, H. Fu, C. Yang, L. Zhao, *J. Energy Chem.* **2022**, *64*, 335.
[17] H. A. Jahn, E. Teller, *Proc. R. Soc. Lond.* **1937**, *161*, 220.
[18] H. A. Jahn, *Proc. R. Soc. Lond. A* **1938**, *164*, 117.
[19] I. B. Bersuker, *Chem. Rev.* **2021**, *121*, 1463.
[20] J. B. Goodenough, *Annu. Rev. Mater. Sci.* **1998**, *28*, 1.
[21] H. Y. Asl, A. Manthiram, *Science* **2020**, *369*, 140.
[22] X. Ma, H. Chen, G. Ceder, *J. Electrochem. Soc.* **2011**, *158*, A1307.
[23] A. Yamada, M. Tanaka, K. Tanaka, K. Sekai, *J. Power Sources* **1999**, *81–82*, 73.
[24] R. J. Gummow, A. de Kock, M. M. Thackeray, *Solid State Ion* **1994**, *69*, 59.
[25] S. K. Ghosh, *ACS Omega* **2020**, *5*, 25493.
[26] C. A. Marianetti, D. Morgan, G. Ceder, *Phys. Rev. B* **2001**, *63*, 224304.
[27] G. Ceder, S. K. Mishra, *Electrochem. Solid State Lett.* **1999**, *2*, 550.
[28] T. Amriou, B. Khelifa, H. Aourag, S. M. Aouadi, C. Mathieu, *Mater. Chem. Phys.* **2005**, *92*, 499.
[29] C. Delmas, C. Fouassier, P. Hagenmuller, *Physica B+C* **1980**, *99*, 81.
[30] B. Ammundsen, J. Paulsen, *Adv. Mater.* **2001**, *13*, 943.
[31] S.-T. Myung, S. Komaba, N. Kumagai, *Chem. Lett.* **2001**, *30*, 80.
[32] R. J. Gummow, D. C. Liles, M. M. Thackeray, *Mater. Res. Bull.* **1993**, *28*, 1249.
[33] X. Y. Tu, K. Y. Shu, *J. Solid State Electrochem.* **2008**, *12*, 245.
[34] J.-M. Kim, H.-T. Chung, *J. Power Sources* **2003**, *115*, 125.
[35] J. Reed, G. Ceder, *Chem. Rev.* **2004**, *104*, 4513.
[36] J. B. Goodenough, K. S. Park, *J. Am. Chem. Soc.* **2013**, *135*, 1167.
[37] M. D. Radin, S. Hy, M. Sina, C. Fang, H. Liu, J. Vinckeviciute, M. Zhang, M. S. Whittingham, Y. S. Meng, A. Van der Ven, *Adv. Energy Mater.* **2017**, *7*, 1602888.
[38] M. M. Thackeray, J. R. Croy, E. Lee, A. Gutierrez, M. He, J. S. Park, B. T. Yonemoto, B. R. Long, J. D. Blauwkamp, C. S. Johnson, Y. Shin, W. I. F. David, *Sustain. Energy Fuels* **2018**, *2*, 1375.
[39] J. Choa, M. M. Thackeray, *J. Electrochem. Soc.* **1999**, *146*, 3577.
[40] R. Benedek, *J. Phys. Chem. C* **2017**, *121*, 22049.
[41] M. H. Rossouw, M. M. Thackeray, *Mater. Res. Bull.* **1991**, *26*, 463.
[42] D.-H. Seo, J. Lee, A. Urban, R. Malik, S. Kang, G. Ceder, *Nat. Chem.* **2016**, *8*, 692.
[43] E. Hu, X. Yu, R. Lin, X. Bi, J. Lu, S. Bak, K.-W. Nam, H. L. Xin, C. Jaye, D. A. Fischer, K. Amine, X.-Q. Yang, *Nat. Energy* **2018**, *3*, 690.
[44] E. Boivin, R. A. House, M. A. Pérez-Osorio, J.-J. Marie, U. Maitra, G. J. Rees, P. G. Bruce, *Joule* **2021**, *5*, 1267.
[45] X. Cao, H. Li, Y. Qiao, M. Jia, X. Li, J. Cabana, H. Zhou, *Adv. Mater.* **2021**, *33*, 2004280.
[46] Z. Lu, S. Hao, Z. Wang, H. Kim, C. Wolverton, *Chem. Mater.* **2024**, *36*, 6381.
[47] N. Yabuuchi, K. Kubota, M. Dahbi, S. Komaba, *Chem. Rev.* **2014**, *114*, 11636.
[48] J.-Y. Hwang, S.-T. Myung, Y.-K. Sun, *Chem. Soc. Rev.* **2017**, *46*, 3529.
[49] J. Billaud, R. J. Clément, A. R. Armstrong, J. Canales-Vázquez, P. Rozier, C. P. Grey, P. G. Bruce, *J. Am. Chem. Soc.* **2014**, *136*, 17243.
[50] M. Shishkin, S. Kumakura, S. Sato, K. Kubota, S. Komaba, H. Sato, *Chem. Mater.* **2018**, *30*, 1257.
[51] R. J. Clément, P. G. Bruce, C. P. Grey, *J. Electrochem. Soc.* **2015**, *162*, A2589.
[52] B. Xiao, X. Liu, M. Song, X. Yang, F. Omenya, S. Feng, V. Sprenkle, K. Amine, G. Xu, X. Li, D. Reed, *Nano Energy* **2021**, *89*, 106371.
[53] C. Zhao, Z. Yao, Q. Wang, H. Li, J. Wang, M. Liu, S. Ganapathy, Y. Lu, J. Cabana, B. Li, X. Bai, A. Aspuru-Guzik, M. Wagemaker, L. Chen, Y.-S. Hu, *J. Am. Chem. Soc.* **2020**, *142*, 5742.
[54] K. Kubota, M. Miyazaki, E. J. Kim, H. Yoshida, P. Barpanda, S. Komaba, *J. Mater. Chem. A* **2021**, *9*, 26810.
[55] X. Chen, Y. Wang, K. Wiaderek, X. Sang, O. Borkiewicz, K. Chapman, J. LeBeau, J. Lynn, X. Li, *Adv. Funct. Mater.* **2018**, *28*, 1805105.
[56] W. Zuo, X. Liu, J. Qiu, D. Zhang, Z. Xiao, J. Xie, F. Ren, J. Wang, Y. Li, G. F. Ortiz, W. Wen, S. Wu, M.-S. Wang, R. Fu, Y. Yang, *Nat. Commun.* **2021**, *12*, 4903.
[57] W. Zuo, Y. Yang, *Acc. Mater. Res.* **2022**, *3*, 709.
[58] N. Yabuuchi, M. Kajiyama, J. Iwatate, H. Nishikawa, S. Hitomi, R. Okuyama, R. Usui, Y. Yamada, S. Komaba, *Nat. Mater.* **2012**, *11*, 512.
[59] S. Kumakura, Y. Tahara, K. Kubota, K. Chihara, S. Komaba, *Angew. Chem., Int. Ed.* **2016**, *55*, 12760.
[60] X. Wu, G.-L. Xu, G. Zhong, Z. Gong, M. J. McDonald, S. Zheng, R. Fu, Z. Chen, K. Amine, Y. Yang, *ACS Appl. Mater. Interfaces* **2016**, *8*, 22227.
[61] W. Zuo, J. Qiu, X. Liu, B. Zheng, Y. Zhao, J. Li, H. He, K. Zhou, Z. Xiao, Q. Li, G. F. Ortiz, Y. Yang, *Energy Storage Mater.* **2020**, *26*, 503.
[62] A. Caballero, L. Hernán, J. Morales, L. Sánchez, J. S. Pena, M. A. G. Aranda, *J. Mater. Chem.* **2002**, *12*, 1142.
[63] Y. Liu, X. Fang, A. Zhang, C. Shen, Q. Liu, H. A. Enaya, C. Zhou, *Nano Energy* **2016**, *27*, 27.
[64] P.-F. Wang, Y. You, Y.-X. Yin, Y.-S. Wang, L.-J. Wan, L. Gu, Y.-G. Guo, *Angew. Chem., Int. Ed.* **2016**, *55*, 7445.
[65] P.-F. Wang, H.-R. Yao, X.-Y. Liu, J.-N. Zhang, L. Gu, X.-Q. Yu, Y.-X. Yin, Y.-G. Guo, *Adv. Mater.* **2017**, *29*, 1700210.
[66] H. Kim, D. H. Seo, J. C. Kim, S.-H. Bo, L. Liu, T. Shi, G. Ceder, *Adv. Mater.* **2017**, *29*, 1702480.
[67] K. Lei, Z. Zhu, Z. Yin, P. Yan, F. Li, J. Chen, *Chem* **2019**, *5*, 3220.
[68] X. Zhang, Z. Wei, K. N. Dinh, N. Chen, G. Chen, F. Du, Q. Yan, *Small* **2020**, *16*, 2002700.
[69] W. Li, Z. Bi, W. Zhang, J. Wang, R. Rajagopalan, Q. Wang, D. Zhang, Z. Li, H. Wang, B. Wang, *J. Mater. Chem. A* **2021**, *9*, 8221.
[70] Y. Zheng, H. Xie, J. Li, K. S. Hui, Z. Yu, H. Xu, D. A. Dinh, Z. Ye, C. Zha, K. N. Hui, *Adv. Energy Mater.* **2024**, *14*, 2400461.
[71] K. Wang, H. Zhuo, J. Wang, F. Poon, X. Sun, B. Xiao, *Adv. Funct. Mater.* **2023**, *33*, 2212607.
[72] R. Prasad, R. Benedek, M. M. Thackeray, *Phys. Rev. B* **2005**, *71*, 134111.
[73] F. Kong, R. C. Longo, D.-H. Yeon, J. Yoon, J.-H. Park, C. Liang, K. C. Santosh, Y. Zheng, S.-G. Doo, K. Cho, *J. Phys. Chem. C* **2015**, *119*, 21904.
[74] K. Hoang, *Phys. Rev. Mater.* **2017**, *1*, 075403.
[75] J. Song, H. Wang, Y. Zuo, K. Zhang, T. Yang, Y. Yang, C. Gao, T. Chen, G. Feng, Z. Jiang, W. Xiao, T. Luo, D. Xia, *Electrochem. Energy Rev.* **2023**, *6*, 20.
[76] H. Chen, X. Xia, J. Ma, *ChemSusChem* **2024**, *17*, 202401120.
[77] N. Ortiz-Vitoriano, N. E. Drewett, E. Gonzalo, T. Rojo, *Energy Environ. Sci.* **2017**, *10*, 1051.

[78] C. Zuo, Z. Hu, R. Qi, J. Liu, Z. Li, J. Lu, C. Dong, K. Yang, W. Huang, C. Chen, Z. Song, S. Song, Y. Yu, J. Zheng, F. Pan, *Adv. Energy Mater.* **2020**, *10*, 2000363.
[79] J. Reed, G. Ceder, *Electrochem. Solid-State Lett.* **2002**, *5*, A145.
[80] H.-S. Park, S.-J. Hwang, J.-H. Choy, *J. Phys. Chem. B* **2001**, *105*, 4860.
[81] L. Mu, S. Xu, Y. Li, Y.-S. Hu, H. Li, L. Chen, X. Huang, *Adv. Mater.* **2015**, *27*, 6928.
[82] W. Zuo, F. Ren, Q. Li, X. Wu, F. Fang, X. Yu, H. Li, Y. Yang, *Nano Energy* **2020**, *78*, 105285.
[83] Z. Xiao, F. Xia, L. Xu, X. Wang, J. Meng, H. Wang, X. Zhang, L. Geng, J. Wu, L. Mai, *Adv. Funct. Mater.* **2022**, *32*, 2108244.
[84] M. Holzapfel, O. Proux, P. Strobel, C. Darie, M. Borowski, M. Morcrette, *J. Mater. Chem.* **2004**, *14*, 102.
[85] M.-H. Cao, Y. Wang, Z. Shadike, J.-L. Yue, E. Hu, S.-M. Bak, Y.-N. Zhou, X.-Q. Yang, Z.-W. Fu, *J. Mater. Chem. A* **2017**, *5*, 5442.
[86] A. Gutierrez, N. A. Benedek, A. Manthiram, *Chem. Mater.* **2013**, *25*, 4010.
[87] A. M. Abakumov, S. S. Fedotov, E. V. Antipov, J.-M. Tarascon, *Nat. Commun.* **2020**, *11*, 4976.
[88] Y. Mahara, N. Nagasako, H. Oka, Y. Kondo, S. Kosaka, H. Nakano, T. Nonaka, Y. Makimura, *ACS Appl. Mater. Interfaces* **2022**, *14*, 24321.
[89] W.-J. Shi, Y.-W. Yan, C. Chi, X.-T. Ma, D. Zhang, S.-D. Xu, L. Chen, X.-M. Wang, S.-B. Liu, *J. Power Sources* **2019**, *427*, 129.
[90] B. K. Ganesan, Y.-S. Lee, *ACS Appl. Energy Mater.* **2023**, *6*, 960.
[91] Y.-S. Xu, M.-Y. Qi, Q.-H. Zhang, F.-Q. Meng, Y.-N. Zhou, S.-J. Guo, Y.-G. Sun, L. Gu, B.-B. Chang, C.-T. Liu, A.-M. Cao, L.-J. Wan, *ACS Appl. Mater. Interfaces* **2022**, *14*, 13379.
[92] Y. Son, D. T. Nguyen, Y. Lee, *J. Power Sources* **2022**, *533*, 231395.
[93] F. Wang, P. Zuo, Z. Xue, Y. Liu, C. Wang, G. Chen, *ACS Energy Lett.* **2024**, *9*, 1249.
[94] H. Ji, J. Wu, Z. Cai, J. Liu, D.-H. Kwon, H. Kim, A. Urban, J. K. Papp, E. Foley, Y. Tian, M. Balasubramanian, H. Kim, R. J. Clément, B. D. McCloskey, W. Yang, G. Ceder, *Nat. Energy* **2020**, *5*, 213.
[95] X. Zhu, F. Meng, Q. Zhang, L. Xue, H. Zhu, S. Lan, Q. Liu, J. Zhao, Y. Zhuang, Q. Guo, B. Liu, L. Gu, X. Lu, Y. Ren, H. Xia, *Nat. Sustain.* **2021**, *4*, 392.
[96] L. Yang, Z. Liu, X. Shen, S. Li, Z. Hu, Q. Kong, J. Ma, J. Li, H.-J. Lin, C.-T. Chen, J.-M. Chen, S.-C. Haw, X. Wang, R. Yu, Z. Wang, L. Chen, *Energy Storage Mater.* **2022**, *44*, 231.
[97] D. Wang, Y.-P. Deng, Y. Liu, Y. Jiang, B. Zhong, Z. Wu, X. Guo, Z. Chen, *Nano Energy* **2023**, *110*, 108340.
[98] P. Hou, M. Dong, Z. Lin, Z. Sun, M. Gong, F. Li, X. Xu, *ACS Sustainable Chem. Eng.* **2023**, *11*, 10785.
[99] Y. Tang, Q. Zhang, W. Zuo, S. Zhou, G. Zeng, B. Zhang, H. Zhang, Z. Huang, L. Zheng, J. Xu, W. Yin, Y. Qiu, Y. Xiao, Q. Zhang, T. Zhao, H.-G. Liao, I. Hwang, C.-J. Sun, K. Amine, Q. Wang, Y. Sun, G.-L. Xu, L. Gu, Y. Qiao, S.-G. Sun, *Nat. Sustain.* **2024**, *7*, 348.
[100] H. Wang, H. Peng, Z. Xiao, R. Yu, F. Liu, Z. Zhu, L. Zhou, J. Wu, *Energy Storage Mater.* **2023**, *58*, 101.

Johan Nguyen obtained his Ph.D degree in chemical engineering from Kangwon National University, Republic of Korea, in 2014. He is currently a research scientist at Leidos after his postdoc at the University of Central Florida. His research interests include the synthesis-characterization-performance relationship of functional heterogeneous materials in energy conversion and storage.

Youngil Lee is currently a full professor at the University of Ulsan. He received his Ph.D degree from Louisiana State University in 1994. He is committed to the research and development of advanced materials and energy storage devices, especially for next-generation high-energy-density batteries.

Yang Yang studied materials science & engineering and obtained his Ph.D. from Tsinghua University in 2010. From 2010 to 2012 he was supported by the Alexander von Humboldt Postdoctoral Fellowship and worked at the University of Erlangen-Nuremberg, Germany. From 2012 to 2015 he was supported by the Peter M. & Ruth L. Nicholas Postdoctoral Fellowship and worked at the Richard E. Smalley Institute for Nanoscale Sci. & Tech., Rice University. Since 2015 he has been a principal investigator at the NanoScience Technology Center and Department of Materials Science & Engineering, University of Central Florida. His current research interests cover materials science, nanomanufacturing of metallic and carbon materials, interface engineering of energy materials, energy conversion and storage devices with a particular focus on aqueous electrochemical systems such as aqueous batteries, fuel cells, electrolyzers for H_2 production and CO_2 reduction.